Interaction of Hydrogen with Actinide Dioxide (011) Surfaces

James T. Pegg,[1,2*] Ashley E. Shields,[3] Mark T. Storr,[2] David O. Scanlon,[1,4] and Nora H. de Leeuw.[1,5*]

[1] Department of Chemistry, University College London, 20 Gordon Street, London WC1H 0AJ, United Kingdom.

[2] Atomic Weapons Establishment (AWE) Plc, Aldermaston, Reading, RG7 4PR, UK.

[3] Oak Ridge National Laboratory, One Bethel Valley Road, Oak Ridge, Tennessee 37831, USA

[4] Diamond Light Source Ltd., Diamond House, Harwell Science and Innovation Campus, Didcot, Oxfordshire OX11 0DE, United Kingdom.

[5] School of Chemistry, University of Leeds, Leeds LS2 9JT, United Kingdom; n.h.deleeuw@leeds.ac.uk

Keywords: Nuclear Fuel, Actinide Dioxide, Noncollinear Magnetism, DFT, Hydrogen Interaction.

Abstract: The corrosion and oxidation of actinide metals, leading to the formation of metal-oxide surface layers with the catalytic evolution of hydrogen, impacts the management of nuclear materials. Here, the interaction of hydrogen with actinide dioxide (AnO_2, An = U, Np, Pu) (011) surfaces by Hubbard corrected Density Functional Theory (PBEsol+U) has been studied, including spin-orbit interactions and non-collinear 3k anti-ferromagnetic behaviour. The actinide dioxides crystalize in the fluorite-type structure, and although the (111) surface dominates the crystal morphology, the (011) surface energetics may lead to more significant interaction with hydrogen. The dissociative adsorption of hydrogen on the UO_2 (0.44 eV), NpO_2 (-0.47 eV), and PuO_2 (-1.71 eV) (011) surfaces has been calculated. It if found that hydrogen dissociates on the PuO_2 (011) surface; however, UO_2 (011) and NpO_2 (011) surfaces are relatively inert. Recombination of hydrogen ions is likely to occur on the UO_2 (011) and NpO_2 (011) surfaces, whereas hydroxide formation is shown to occur on the PuO_2 (011) surface, which distorts the surface structure.

1 INTRODUCTION

To minimise issues with nuclear interdiction and enable the recycling of decommissioned armaments, the conversion of classified actinide materials to commercial reactor-grade fuels is of considerable interest. The radiolysis of water and organic matter causes the evolution of hydrogen gas [1, 2] and the hydrogen-catalysed oxidative corrosion of actinide metals remains an important field. Incidents involving uncontrolled corrosion have resulted in: the formation of incondensable gases, the expansion of solids, and thermal excursions.[3-6] To reduce the risk of containment failure and conduct environmental assessments, it is important to gain insight into the interaction of hydrogen with nuclear materials.[7] To compensate for known experimental issues (radiogenic nature, impurity phases, legal constraints), computational methods offer a complementary means of investigation.[8-14]

The unavoidable oxidation of the actinide metals forms an actinide dioxide (AnO_2) surface layer, where changes in the electronic and magnetic structure impact successive corrosion reactions.[15] The actinides are non-trivial highly correlated electron systems, where conventional computational methods often fail to describe the electromagnetic structure. To model actinide systems, a number of methods have been used: the self-interaction correction (SIC) method,[16] Hubbard modified Density Functional Theory (DFT+U),[17-21] hybrid density functionals,[22-25] and dynamic mean field theory (DMFT). The computational expense of these methods is far from equal,[26] and as a computationally tractable means of investigation, DFT+U is especially useful for periodic calculations, as the most advantageous methods also depend on the model geometry..[14] The importance of including non-collinear magnetic behaviour and spin-orbit interactions (SOI) to correctly describe the electronic structure has been highlighted in the literature.[8-11, 27, 28] In earlier hybrid investigations of the magnetic strucutre, the PBEsol functional with an appropriate U correction has shown comparable results. For instance, in studies comparing DFT+U with HSE06 calculations, transverse 3k AFM (UO_2, NpO_2) and longitudinal 3k AFM (PuO_2) states have been identified.[9-11, 29, 30]

The inclusion of relativistic effects is computationally expensive, and scalar collinear calculations are often used to approximate the electronic structure.[31] For instance, the dissociative adsorption (-5.15 eV) and molecular dissociation (0.48 eV) energy has been calculated for hydrogen from non-relativistic scalar DFT+U PuO_2 (011) models.[32, 33] However, the findings are incomplete and the chemisorption energy is exceptionally exothermic; a non-collinear relativistic treatment of actinide systems is therefore needed to

obtain accurate surface energetics.[9] It has been shown that the magnetic order of the actinide oxides greatly impacts their surface energetics [8-11], and the interaction of hydrogen therefore needs to be recalculated considering non-collinear relativistic contributions. Other studies on AnO_2 interstitial sites have considered the interaction of hydrogen.[34-43] The behaviour was found to be complex and controlled by the actinide element. In the early actinides with itinerant 5f-electrons, hydrogen occupied interstitial octahedral sites, whereas in the late actinides with localised 5f-electrons, hydroxyl groups are formed from hydrogen.[34, 35] A number of studies contrast actinide oxide behaviour with isostructural cerium dioxide (CeO_2), however the relatively simplistic electronic structure of cerium is not directly comparable.[44]

In this paper, the interaction of hydrogen with the AnO_2 (An = U, Np, Pu) (011) surface has been investigated by DFT+U, including relativistic effects. Earlier work has shown that the dissocation of molecular H_2 does not occur on the (111) surface;[45] however, the (011) surface offers an energetically less stable and more reactive substrate. Therefore, the following work complements and contrasts with the earlier study on AnO_2 (111) surface investigations.[45] To accurately represent the surface structure within the limits of computational resources, non-collinear 3k AFM behaviour and SOI are implemented throughout the study.

2 COMPUTATIONAL METHODOLOGY

2.1 Calculation Details

The interaction of hydrogen with AnO_2 (011) surfaces has been calculated with the Vienna Ab-initio Simulation Package (VASP).[16, 26, 46] The code uses relativistic effective core potentials (ECPs), the frozen-core projector-augmented wave (PAW) method, and a planewave basis set.[23, 47] A planewave basis set cut-off energy of 500 eV has been used. The explicit valence electrons included: hydrogen ($1s^1$), oxygen ($2s^2$, $2p^4$), uranium ($6s^2$, $7s^2$, $6p^6$, $6d^2$ $5f^2$), neptunium ($6s^2$, $7s^2$, $6p^6$, $6d^2$ $5f^3$), and plutonium ($6s^2$, $7s^2$, $6p^6$, $6d^2$ $5f^4$). To improve on earlier functionals that calculate the exchange correlation energy, the revised Perdew-Burke-Ernzerhof for solids (PBEsol) functional has been used.[8, 48, 49] The iteration thresholds for the electronic ($1 \cdot 10^{-5}$ eV) and ionic ($1 \cdot 10^{-2}$ eV·Å^{-1}) convergence are shown. The code by Henkleman et al. [50-52] was used (See Supporting Information) for the Bader charge analysis.[53]

To compensate for the highly correlated nature of the AnO_2 systems via the Liechtenstein et al. formulism, the on-site Coulomb repulsion of An 5f-electrons is treated with Coulomb (U) and exchange (J) modifiers: [17-21]

$$E_{dc}(\hat{n}) = \frac{U}{2}\hat{n}_{tot}(\hat{n}_{tot} - 1) - \frac{J}{2}\sum_{\sigma}\hat{n}^{\sigma}_{tot}(\hat{n}^{\sigma}_{tot} - 1) \quad (1)$$

The double counting energy term (E_{dc}), the on-site occupancy matrix (n), and the spin index (σ) are shown. The method is identical to the Dudarev et al. formulism when J = 0.00 eV; however, J has been shown to increase f-electron anisotropy.[8, 19, 54, 55] A transverse 3k AFM state for UO_2 (U = 3.35 eV, J = 0.00 eV) and NpO_2 (U = 4.25 eV, J = 0.00 eV) model is used; whereas, a longitudinal 3k AFM for PuO_2 (U = 6.00 eV, J = 0.00 eV) model was used.[9-11] The results can be compared directly with our earlier investigations.[45]

The surface models have been constructed from the methodology described in our earlier work.[9] An ionically relaxed bulk cell has been used to construct the non-dipolar AnO_2 (011) surface with the METADISE code,[56] which considers the surface as a series of stacked planes. The low-index AnO_2 (011) model employed herein is a slab comprised of 7 monolayers and to isolate the surface from its periodic image, a vacuum gap of 20 Å was used.[57, 58] The integration of the Brillouin zone was calculated by a $4 \cdot 4 \cdot 1$ Γ-centred k-point grid with the Gaussian method[9, 59] and all models have considered SOI.[60] The spin quantisation axis is defined by (0, 0, 1) plane, from which magnetic and spinor-like values are calculated. Full ionic relaxation of the surfaces was carried out and the density of states have been illustrated by the SUMO code, a command-line plotting tool for ab-initio calculations.[61] The electronic structure of the clean AnO_2 (011) surface can be found in the Supplementary Online Material. The methodology employed is consistent throughout this work.

2.2 Inequivalent Positions

The dissociative adsorption and molecular adsorption of hydrogen on the AnO_2 (011) surfaces must be considered for multiple inequivalent lattice sites, where the effect of magnetic inequivalence is assumed to be negligible (**Figure 1**). The ions superior (s) or inferior (I) to the

plane of the surface are designated by the relevant subscripts, where the plane of the surface bisects the O_S^{2-} ions.[45]

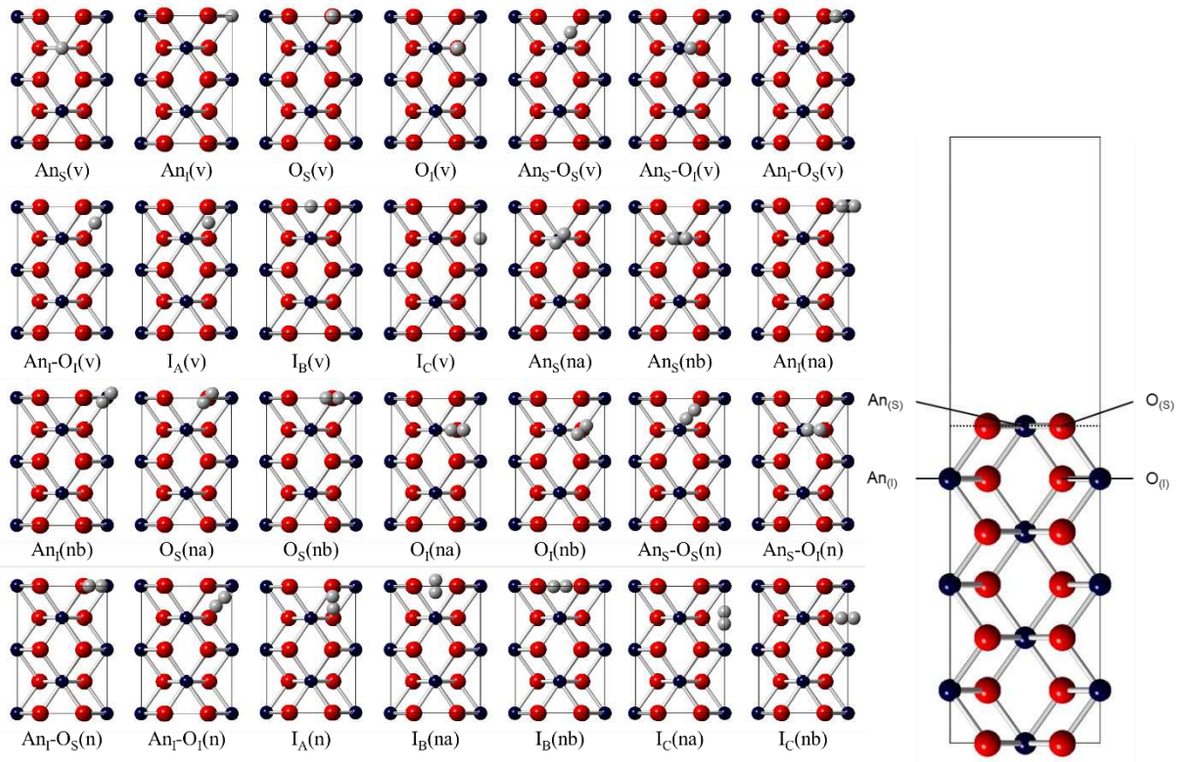

Figure 1: a) Plan view of the initial inequivalent configurations of the dissociative atomic and molecular hydrogen on the AnO_2 (011) surface. The An^{4+} (blue) and O^{2-} (red) ions are indicated. The individual hydrogen positions are shown in grey. The minimum distance of the hydrogen atoms above the plane of the surface is 1 Å. The hydrogen molecule is considered with either orthogonal (v) or parallel (n) orientations relative to the surface plane. b) Side view of the low-index AnO_2 (011) surface. The An^{4+} (blue) and O^{2-} (red) ions are indicated by the colours in the parentheses. The surface plane bisects the Os^{2-} ions as illustrated by the dashed black line. Ionic sites are differentiated, either as superior ($_S$) or inferior ($_I$), by their position relative to the plane of the surface.

The inequivalent sites of interest on the AnO_2 (011) surface include: four on-top atomic (An_S, An_I, O_S, O_I) positions, four bridging (An_S-O_S, An_S-O_I, An_I-O_S, An_I-O_I) and three interstitial (I_A, I_B, I_C) sites. The orientation relative to the plane of the surface of molecular H_2 has been considered as either orthogonal to the surface (v), or parallel to the surface along the direction of a bond (n). Initially, hydrogen was placed at a minimum of 1 Å above the plane of the surface. The ionic coordinates, magnetic vectors, and dimensions of the unit cell can be found in the Supplementary Online Material.

2.3 Hydrogen Adsorption

The hydrogen adsorption energy (E_{ads}) has been calculated from the: total energy of the surface with the adsorbate ($E_{slab+absorbate}$), the energy of the adsorbate ($E_{absorbate}$), and the energy of the clean (adsorbate-free) surface (E_{slab}). To avoid the formation of a dipole during adsorption, hydrogen is adsorbed at equivalent sites on both sides of the slabs.

$$E_{ads} = 0.5[E_{slab+absorbate} - (E_{slab} + E_{absorbate})] \quad (2)$$

The energy of the hydrogen adsorbate ($E_{absorbate}$) has been calculated in an earlier PBEsol study, where the H_2 molecule was modelled in isolation in a 10 $Å^3$ cubic unit cell.[45] The difference in dissociation energy between experiment and computation (relative to the energy of chemisorption) was found to be negligible.[45, 62, 63]

3 RESULTS & DISCUSSION

3.1 Uranium Dioxide

The dissociative adsorption of hydrogen on the UO_2 (011) surface (as with the UO_2 (111) surface) is endothermic (**Figure 2**). In the $aH_{(011)}$ configuration, (E_{ads} = 1.13 eV), atomic hydrogen is located 2.044 Å from the U_S ion; whereas, in the $bH_{(011)}$ configurations (E_{ads} = 1.45 eV), atomic hydrogen is located 2.092 Å from the U_S ion. In the high-energy $cH_{(011)}$ configuration, atomic hydrogen is located within the I_C interstitial channel, which offers a means by which hydrogen ions might diffuse across the surface. The minimum U_I-H (2.250 Å), O_S-H (2.317 Å), and O_I-H (2.258 Å) distances have been calculated.

The formation of the U f-defect state near the conduction band minimum (CBM) and the absence of hybrid H s- and O p-states in the high-energy a-$cH_{(011)}$ configurations is indicative of the oxidation of the U^{4+} ion to a U^{5+} ion and the existence of a hydride group, which is confirmed by the Bader charge distribution (Supplementary Online Material). As the a-$cH_{(011)}$ configurations are energetically unfavourable, a hydride-induced corrosion mechanism by the UO_2 (011) surface seems improbable.[34, 64-66]

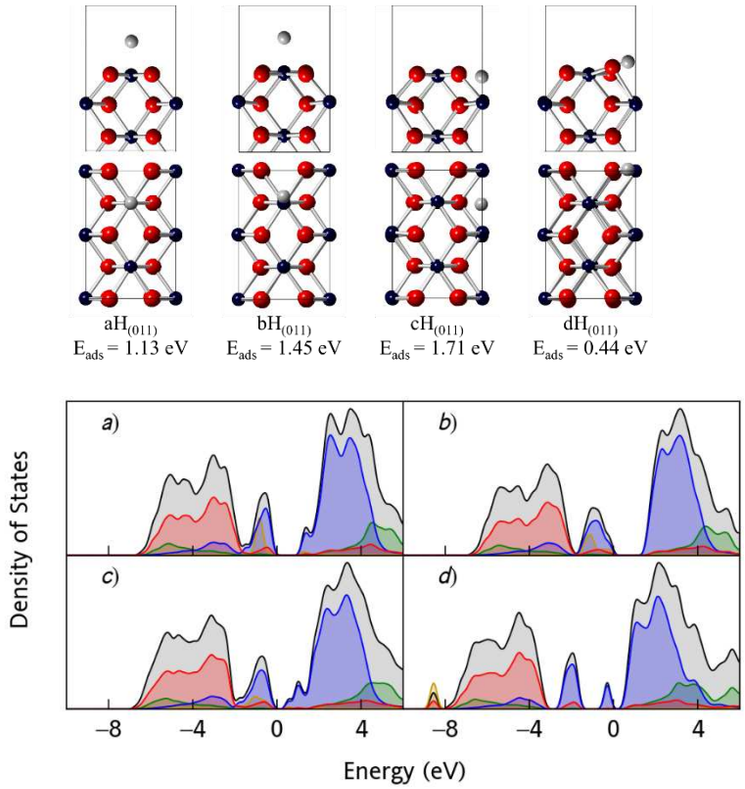

Figure 2: Upper figure: Side (top) and plan (bottom) views of the dissociative adsorption sites of atomic H on the UO_2 (011) surface, U^{4+} (blue), O^{2-} (red) and H (grey), also indicating the energies of adsorption (E_{ads}). Lower figure: Density of states of the a-$dH_{(011)}$ configurations for the UO_2 (011) surface; total density of states (black), U f- (blue), U d- (green), O p- (red), and H s- (yellow) bands are coloured. The labelling in the density of states (a-d) corresponds to the individual adsorption sites. The Fermi level is set at 0.00 eV. Note: the hydrogen s-band has been magnified by a factor of 40 for clarity.

The s-band located close to the valence band maximum (VBM) indicates physisorption for the a-$cH_{(011)}$ configurations; whereas, the s-band located at the lower -8 eV to -9 eV range indicates chemisorption for the $dH_{(011)}$ configuration. In the lower-energy $dH_{(011)}$ configuration, the hydrogen atom is positioned along the U_I-O_S bond. The surface undergoes considerable distortion, causing an increase in the U_S-O_S bond distance from 2.313 Å to 2.446 Å. The minimum U_I-H (2.644 Å) and O_S-H (0.995 Å, reminiscent of an OH group) distances have been calculated. The surface rearrangement is limited to the first monolayer and is not seen in the sub-surface layers. The density of states (DoS) shows an U f-defect (reduction of U^{4+} to U^{3+}) and hybrid H s-states with O p-states (OH formation), where a protonic state and the reduction of the U (b) ion is confirmed by the Bader charge analysis (Supplementary Online Material).

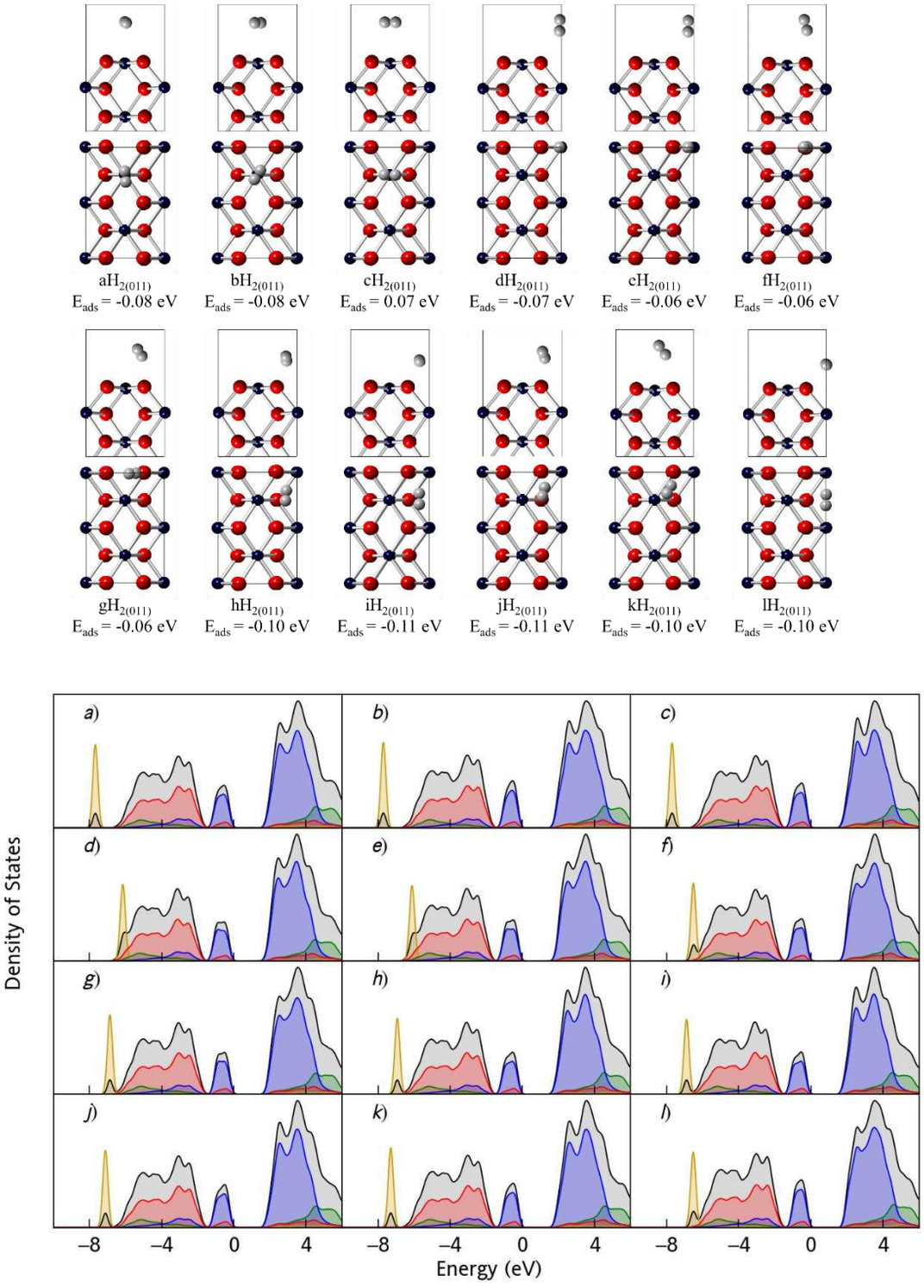

Figure 3: Upper figure: Side (top) and plan (bottom) views of the adsorption sites of molecular H_2 on the UO_2 (011) surface, U^{4+} (green), O^{2-} (red) and H (grey), also indicating the energies of adsorption (E_{ads}). Lower figure: Density of states of the a-l$H_{2(011)}$ configurations for the UO_2 (011) surface; total density of states (black), U f- (blue), U d- (green), O p- (red), and H s- (yellow). The labelling in the density of states (a-l) corresponds to the

individual adsorption sites. The Fermi level is set at 0.00 eV. Note: the hydrogen s-band has been magnified by a factor of 10 for clarity.

The interaction of molecular H_2 on the UO_2 (011) surface results in 12 distinct a-l$H_{2(011)}$ configurations (**Figure 3**). In each instance, molecular H_2 is physisorbed with adsorption energies in the 0.07 to -0.11 eV energy range. The electronic structure for molecular a-h$H_{2(111)}$ configurations has been calculated, where the absence of defect states or of hybrid H s- and O p-states indicates physisorption. The magnitude of the electrostatic interaction is indicated by the position of the H s-band. In the low-energy i$H_{2(011)}$ configuration, the Bader charge indicates that the H_2 molecule is partially polarised by 0.04 e (See Supplementary Online Material), which is unusual as the hydrogen ions occupy equivalent lattice positions. The observed polarisation of the hydrogen ion could be explained by the inherent magnetism. The individual magnetic moment and chemical bond orientation slightly impacts the local structure; whereby, the accompanying crystallographic distortion produces a local electric polarization.[67]

The dissociation of molecular H_2 on the UO_2 (011) surface is not observed, similar to earlier calculations of hydrogen interaction with the UO_2 (111) surface.[45] Steric hindrance could impede a molecular dissociative mechanisms. It is noted for instance that an OH group is formed with atomic hydrogen on the UO_2 (011) surface, however the dissociative adsorption energy is endothermic. It is therefore probable that thermodynamic factors are the limiting factor.

3.2 Neptunium Dioxide

The interaction of hydrogen with the NpO_2 (011) surface forms a-b$H_{(111)}$ configurations (**Figure 4**). An endothermic adsorption energy (1.86 eV) for the a$H_{(011)}$ configuration has been calculated. Minor hybrid H s- and Np f-defect states are found. The oxidation of Np^{4+} to Np^{5+} (Np^{5+}-H bond length of 2.129 Å) occurs on hydrogen adsorption and the formation of a hydride ion has been confirmed via Bader charge analysis. In contrast to the a$H_{(011)}$ configuration, the adsorption energy for b$H_{(011)}$ is exothermic (-0.47 eV). The formation of an OH group (bond length of 0.997 Å) has been confirmed by Bader charge analysis (H charge of 0.64 e). The formation of the OH group (hybrid H s- and O p- states) and the reduction of Np^{4+} to Np^{5+} (Np f-defect) can be inferred from the DoS. The formation of the Np f-defect results in Mott-Hubbard characteristics.

It is noted that the electronic structure is greatly affected by the adsorbed hydrogen. The epitaxial absorbance measurements of NpO_2 thin films report a band-gap of 2.85 eV,[68] whereas electrical resistivity measurements of NpO_2 report a band-gap of 0.4 eV.[69] The difference between the two measurements has been accredited to the sample preparation methods employed, showing how the inhomogeneity of samples is a major obstacle for experimental measurements of the band structure.

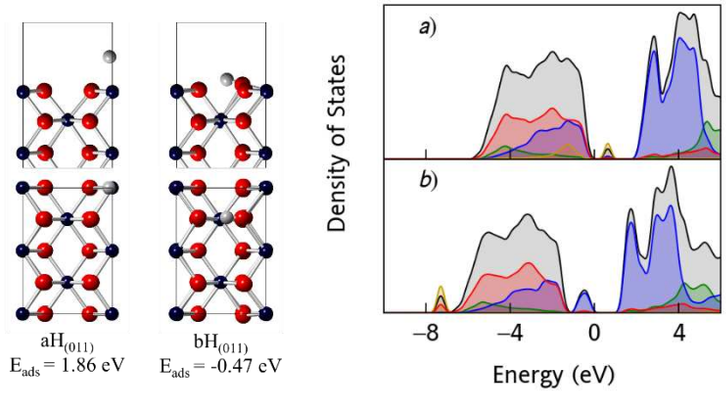

Figure 4: Left figure: Side (top) and plan (bottom) views of the adsorption sites of dissociative atomic H on the NpO_2 (011) surface, Np^{4+} (blue), O^{2-} (red) and H (grey), also indicating the energies of adsorption (E_{ads}). Right figure: Density of states of the a-$bH_{(011)}$ configurations for the NpO_2 (011) surface, total density of states (black), Np f- (blue), Np d- (green), O p- (red), and H s- (yellow) bands. The labelling in the density of states (a-b) corresponds to the individual adsorption sites. The Fermi level is set at 0.00 eV. Note: the hydrogen s-band has been magnified by a factor of 40 for clarity.

The energies of adsorption of molecular H_2 on the NpO_2 (011) surface range from -0.10 eV to -0.06 eV, where 10 distinct a-$jH_{(111)}$ configurations have been identified (**Figure 5**). The adsorption sites include positions: near the Np_S ion (the a-$bH_{2(011)}$), near the Np_I ion (the c-$dH_{2(011)}$), near the O_S ion ($eH_{2(011)}$) and near the O_I ion (f-$hH_{2(011)}$). In the i-$jH_{2011)}$ configurations, molecular H_2 occupies interstitial positions. The position of the H s-band in the DoS reflects the relative adsorption site stability. Notable surface reorganization or molecular H_2 dissociation has not been observed.

The dissociation of molecular H_2 is not observed in the low-energy molecular $fH_{2011)}$ configuration, In the dissociative atomic $bH_{(011)}$ configuration, it is noted that atomic hydrogen binds to form an OH group. It is curious that despite this significant activity, dissociation of

the molecular H_2 is not observed. It is assumed that steric factors may hinder secondary OH group formation, making the dissociation reaction energy barrier too high.

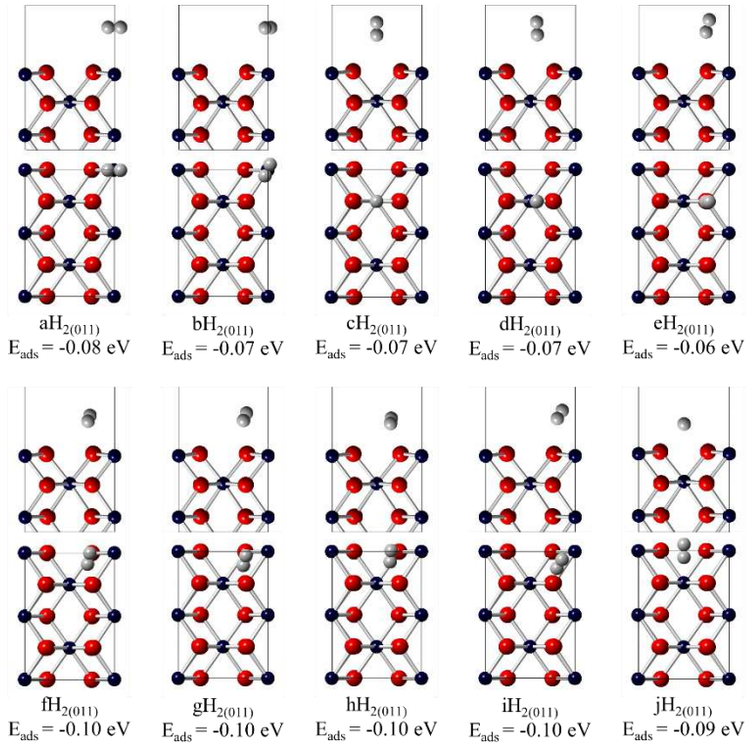

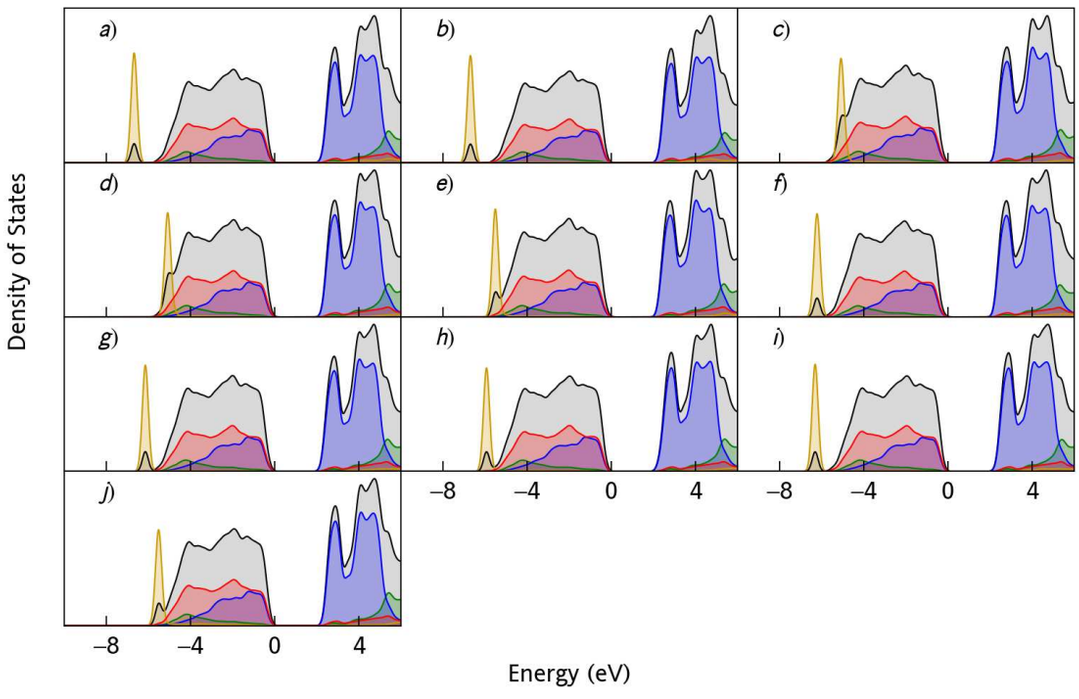

Figure 5: Upper figure: Side (top) and plan (bottom) views of the adsorption sites of molecular H_2 on the NpO_2 (011) surface, Np^{4+} (blue), O^{2-} (red) and H (grey), also indicating the energies of adsorption (E_{ads}). Bottom figure: Density of states of the a-j$H_{2(011)}$ configurations for the NpO_2 (011) surface; total density of states (black), Np f- (blue), Np d- (green), O p- (red), and H s- (yellow) bands. The labelling in the density of states (a-j) corresponds to the individual adsorption sites. The Fermi level is set at 0.00 eV. Note: the hydrogen s-band has been magnified by a factor of 10 for clarity.

3.3 Plutonium Dioxide

The dissociative adsorption of hydrogen on the PuO_2 (011) surface (E_{ads} of -1.71 eV) is exothermic (**Figure 6**). In contrast with dissociative hydrogen adsorption on UO_2 and NpO_2 (011) surfaces, the PuO_2 (011) $aH_{(011)}$ configuration is the only adsorption site, however the increased adsorption site stability is an artefact surface reactivity. The O_S-H bond length (1.00 Å) indicates the formation of an OH group, which is confirmed by the DOS band located at -7 eV to -6 eV, comprised of H s- and O p-states. The number of Pu f-states in the valence band increases, whereas the number of Pu f-states in the conduction band decreases, which indicates that the interaction of hydrogen with the surface causes high-energy Pu f-states to shift to lower energy levels. In addition, the Bader charge distribution indicates that atomic hydrogen exists in a protonic state (Supplementary Online Material), with a corresponding reduction of the Pu(a) ion, whereas the charge of the O ions is only partially increased. The formation of the OH group distorts the PuO_2 (011) surface, increasing the Pu_S-O_S (2.30 Å to 2.44 Å) and Pu_I-O_S (2.23 Å to 2.24 Å) bond lengths. The single dissociative adsorption of hydrogen differs from an earlier study of the PuO_2 (011) surface, where two distinct chemisorption sites with a very large energy difference (-1.695 eV and -5.147 eV) have been described.[32, 33]

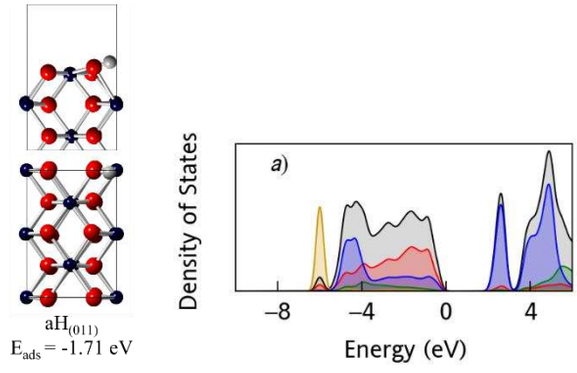

Figure 6: Left figure: Side (top) and plan (bottom) view of the adsorption site of dissociative atomic H on the PuO_2 (011) surface, Pu^{4+} (blue), O^{2-} (red) and H (grey), also indicating the energy of adsorption (E_{ads}). Right figure: Density of states of the $aH_{(011)}$ configuration for the PuO_2 (011) surface; total density of states (black), Pu

f- (blue), Pu d- (green), O p- (red), and H s- (yellow) bands. The labelling in the density of states (a) corresponds to the individual adsorption site. The Fermi level is set at 0.00 eV. Note: the hydrogen s-band has been magnified by a factor of 40 for clarity.

The interaction of molecular H_2 on the PuO_2 (011) surface results in 13 distinct a-m$H_{2(011)}$ configurations (**Figure 7**). A physisorption energy of -0.04 eV to -0.18 eV defines the a-l$H_{2(011)}$ configurations (confirmed by the electronic structure). In the c-d$H_{2(011)}$ configurations (adsorption energies of -0.13 to -0.14 eV), molecular H_2 is located near the Pu_I ion and positioned orthogonal to the surface. As a potential prelude to dissociation of molecular H_2 (owing to the resemblance of this configuration to the a$H_{(011)}$ configuration), molecular H_2 is near the O_S ions in the i-j$H_{2(011)}$ configurations (physisorption energies of -0.10 eV to -0.11 eV). However, molecular H_2 does not dissociate spontaneously from this configuration, probably owing to a high energetic barrier due to by steric forces, which could hinder the dissociation process. Finally, the k-l$H_{2(011)}$ configuration offers another unreactive site located between Pu_I ions.

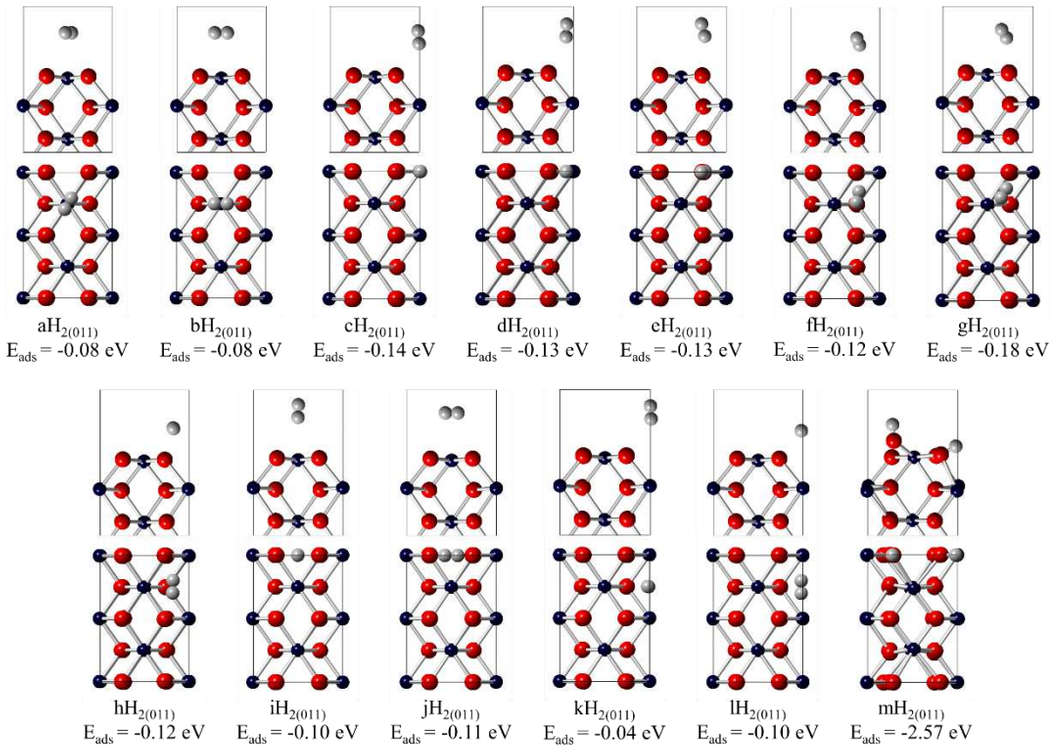

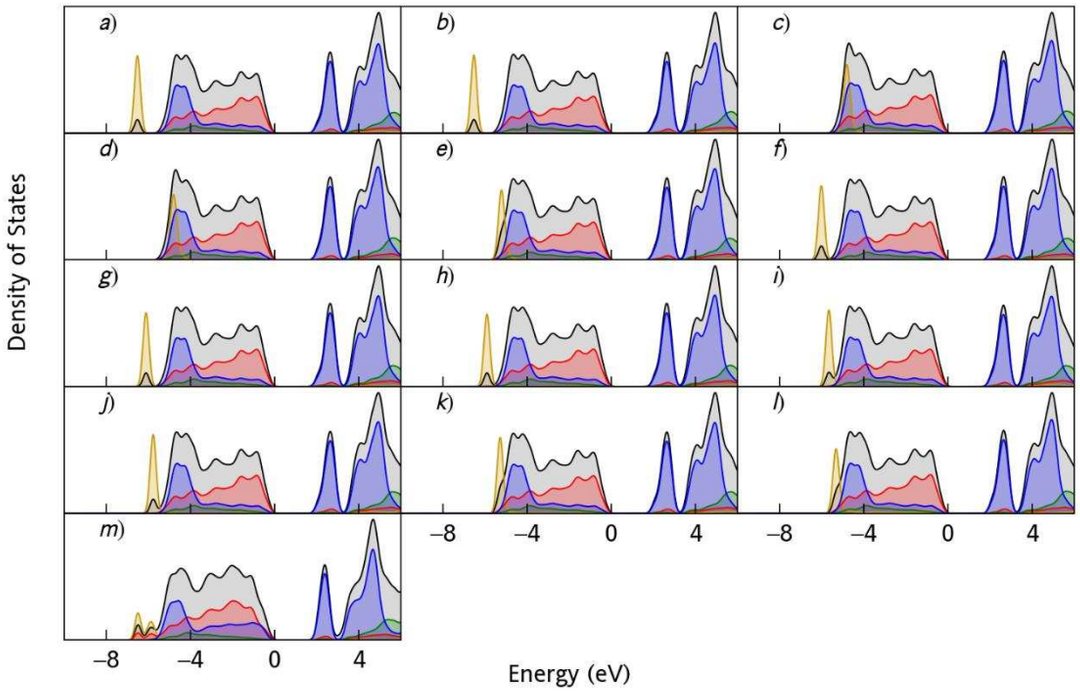

Figure 7: Upper figure: Side (top) and plan (bottom) views of the adsorption sites of molecular H_2 on the PuO_2 (011) surface, Pu^{4+} (blue), O^{2-} (red) and H (grey), also indicating the energies of adsorption (E_{ads}). Bottom figure: Density of states of the a-m$H_{2(011)}$ configurations for the PuO_2 (011) surface; total density of states (black), Pu f- (blue), Pu d- (green), O p- (red), and H s- (yellow) bands. The labelling in the density of states (a-m) corresponds to the individual adsorption sites. The Fermi level is set at 0.00 eV. Note: the hydrogen s-band has been magnified by a factor of 10 for clarity.

The dissociation of molecular H_2 on the PuO_2 (011) surface forms the m$H_{2(011)}$ configuration. Two chemically inequivalent OH groups are found and a chemisorption energy of -2.57 eV has been calculated. To differentiate the chemically inequivalent OH groups, αH (located above the Pu_I ion) and βH (located above the O_S ion) are defined. The atomic a$H_{(011)}$ and O-αH (bond length = 1.011 Å) groups are isostructural; whereas, the O-βH (bond length = 0.975 Å) group is bound orthogonally to the surface plane. The Bader charge of the αH ion is 0.64 e; whereas, the Bader charge of the β-H ion is 0.56 e. The formation of the OH groups shifts Pu 5f-states from the conduction to valence band with a corresponding reduction of the Pu(c) ion, confirmed by Bader charge analysis. Individual hybrid H s- and O p-bands are also located at -6 eV to -7 eV, which confirm the formation of the chemically inequivalent OH groups.

4 CONCLUSIONS

The dissociative and molecular adsorption of hydrogen on the AnO_2 (011) surfaces has been studied, where the models include SOI and non-collinear 3k AFM contributions to obtain accurate structures and energies. The results complement an earlier AnO_2 (111) surface-hydrogen interaction investigation [45]

The nature of the interaction of the hydrogen molecule with the AnO_2 oxides is reasonably complex. On ionic oxides, H_2 can dissociate heterolytically forming a proton on an O ion (OH group) and a hydride on a surface cation (MH). This does not lead to the chemical reduction of the oxide. The other possibility is homolytic dissociation, where two OH groups are formed (adsorbed protons) and the two electrons of the H_2 molecule are transferred to low-lying d or f states of the cations. This leads to a change in oxidation state and a reduction of the oxide. The formation of two OH groups is observed on PuO_2 indicating homolytic dissociation; whereas, the formation of a hydride or of an OH on UO_2 and NpO_2, indicates heterolytic dissociation. The preferential formation of a hydride ion $[(UO_2)_n]^+H^-$ or hydroxide ion $[Pu_nO_{2n-1}]^+[OH]^-$ has been shown earlier.[34] Here, the more itinerant uranium and neptunium 5f electrons enable hydride formation; whereas, the more localized plutonium electrons promote hydroxide formation.

The number of viable adsorption sites decreases along the U-Pu series, corresponding to an increase in surface energies.[9] In each instance, the dissociative adsorption of hydrogen leads to the formation of an OH group with a surface O_S ion. The formation energy across the AnO_2 (011) surfaces changes from endothermic to exothermic: UO_2 (0.44 eV), NpO_2 (-0.47 eV), and PuO_2 (-1.71 eV). The increasing energy along the clean AnO_2 (An = U, Np, Pu) (011) surface offers a simple rationalisation; here, higher-energy surfaces are more readily passivated by hydrogen treatment. In contrast, the endothermic-exothermic transition for OH formation on AnO_2 (111) surfaces has been studied in an earlier investigation; where the energy of adsorption for UO_2 (0.82 eV), NpO_2 (-0.10 eV), and PuO_2 (-1.25 eV) has been calculated.[45] It has been shown that hydrogen dissociation on the AnO_2 (111) surfaces does not occur.

As shown by the relatively higher surface energy compared to the UO_2 and NpO_2 (011) surfaces,[9] the PuO_2 (011) surface is less stable and more reactive, which enables the dissociation of the H_2 molecule with the formation of inequivalent OH groups (bond lengths = 0.975 Å, 1.011 Å). In comparison, molecular H_2 becomes only physisorbed on the PuO_2 (111) surface (of lower surface energy), illustrating the role of surface stabilities, as quantified by the

surface energies, on the dissociation potential.[45] When compared with scalar calculations of hydrogen interactions with the PuO_2 (011) surface,[32, 33] it is clear that our non-collinear relativistic treatment identifies higher binding energies. These results therefore also highlight the challenge of modelling AnO_2 systems with current computational methods.

5 SUPPLEMENTARY INFORMATION

See supplementary material for the following information: Clean surface—fixed unit cell dimensions, ionic positions, magnetic structure, k-point convergence, and electronic density of states, and hydrogen interactions—ionic positions, magnetic structure, and Bader charges.

6 ACKNOWLEDGEMENTS

This research was supported by the UK Engineering & Physical Science Research Council (EPSRC) (Grant nos. EP/G036675 and EP/K016288) and the Atomic Weapons Establishment (AWE). JTP thanks Ornella Romeo for her help and kindness. AES acknowledges the United States Department of Homeland Security (DHS), Domestic Nuclear Detection Office (DNDO), National Technical Nuclear Forensics Centre (NTNFC) for a Postdoctoral Research Fellowship. NHdL thanks the Royal Society for an Industry Fellowship and AWE for a William Penney Fellowship. This work made use of the ARCHER UK National Supercomputing Service (http://www.archer.ac.uk), via our membership of the UK's HEC Materials Chemistry Consortium, which is funded by EPSRC (EP/L000202).

7 DATA AVAILABILITY STATEMENT

The data that supports the findings of this study are available within the article [and its supplementary material].

8 BIBLIOGRAPHY

[1] H.E. Sims, K.J. Webb, J. Brown, D. Morris, R.J. Taylor, Hydrogen yields from water on the surface of plutonium dioxide, J. Nucl. Mater. 437(1) (2013) 359-364.
[2] J. Meesungnoen, J.-P. Jay-Gerin, Radiolysis of supercritical water at 400 °C: Density dependence of the rate constant for the reaction of hydronium ions with hydrated electrons, Phys. Chem. Chem. Phys. (2019).

[3] J.M. Haschke, Corrosion of Uranium in Air and Water Vapor: Consequences for Environmental Dispersal, J. Alloys Compd. 278(1–2) (1998) 149-160.
[4] J.M. Haschke, T.H. Allen, L.A. Morales, Surface and Corrosion Chemistry of Plutonium, Los Alamos Sci. 26 (2000).
[5] J.M. Haschke, T.H. Allen, J.L. Stakebake, Reaction Kinetics of Plutonium with Oxygen, Water and Humid Air: Moisture Enhancement of the Corrosion Rate, J. Alloys Compd. 243(1–2) (1996) 23-35.
[6] J.M. Haschke, J.C. Martz, Catalyzed Corrosion of Plutonium: Hazards and Applications, Los Alamos Sci. 26 (2000).
[7] L. Zhang, B. Sun, Q. Zhang, H. Liu, K. Liu, H. Song, First-Principles Study of the Hydrogen Resistance Mechanism of PuO_2, ACS Omega 5(13) (2020) 7211-7218.
[8] J.T. Pegg, X. Aparicio-Anglès, M. Storr, N.H. de Leeuw, DFT+U Study of the Structures and Properties of the Actinide Dioxides, J. Nucl. Mater. 492 (2017) 269-278.
[9] J.T. Pegg, A.E. Shields, M.T. Storr, D.O. Scanlon, N.H. de Leeuw, Noncollinear Relativistic DFT + U Calculations of Actinide Dioxide Surfaces, J. Phys. Chem. C 123(1) (2019) 356-366.
[10] J.T. Pegg, A.E. Shields, M.T. Storr, A.S. Wills, D.O. Scanlon, N.H. de Leeuw, Hidden Magnetic Order in Plutonium Dioxide Nuclear Fuel, Phys. Chem. Chem. Phys. 20(32) (2018) 20943-20951.
[11] J.T. Pegg, A.E. Shields, M.T. Storr, A.S. Wills, D.O. Scanlon, N.H. de Leeuw, Magnetic Structure of UO_2 and NpO_2 by First-Principle Methods, Phys. Chem. Chem. Phys. 21(2) (2019) 760-771.
[12] A.E. Shields, A Computational Analysis of Thorium Dioxide and $Th_{(1-x)}$ U_xO_2 Systems, UCL (University College London), 2015.
[13] A.E. Shields, D. Santos-Carballal, N.H. de Leeuw, A Density Functional Theory Study of Uranium-Doped Thoria and Uranium Adatoms on the Major Surfaces of Thorium Dioxide, J. Nucl. Mater. 473 (2016) 99-111.
[14] A.E. Shields, A.J. Miskowiec, J.L. Niedziela, M.C. Kirkegaard, K. Maheshwari, M.W. Ambrogio, R.J. Kapsimalis, B.B. Anderson, Shining a light on amorphous U2O7: A computational approach to understanding amorphous uranium materials, Optical Materials 89 (2019) 295-298.
[15] B. Ao, R. Qiu, First-principles explorations of the universal picture of oxide layer structure over metallic plutonium, Corrosion Science (2019).
[16] J.P. Perdew, A. Zunger, Self-Interaction Correction to Density-Functional Approximations for Many-Electron Systems, Phys. Rev. B 23(10) (1981) 5048-5079.
[17] P. Hohenberg, W. Kohn, Inhomogeneous Electron Gas, Phys. Rev. 136(3B) (1964) B864-B871.
[18] W. Kohn, L.J. Sham, Self-Consistent Equations Including Exchange and Correlation Effects, Phys. Rev. 140(4A) (1965) A1133-A1138.
[19] S.L. Dudarev, G.A. Botton, S.Y. Savrasov, C.J. Humphreys, A.P. Sutton, Electron-Energy-Loss Spectra and the Structural Stability of Nickel Oxide: An LSDA+U Study, Phys. Rev. B 57(3) (1998) 1505-1509.
[20] A.I. Liechtenstein, V.I. Anisimov, J. Zaanen, Density-Functional Theory and Strong Interactions: Orbital Ordering in Mott-Hubbard Insulators, Phys. Rev. B 52(8) (1995) R5467-R5470.
[21] V.I. Anisimov, J. Zaanen, O.K. Andersen, Band Theory and Mott Insulators: Hubbard U instead of Stoner I, Phys. Rev. B 44(3) (1991) 943-954.
[22] C. Adamo, V. Barone, Toward Reliable Density Functional Methods without Adjustable Parameters: The PBE0 Model, J. Chem. Phys. 110(13) (1999) 6158-6170.

[23] J. Heyd, G.E. Scuseria, M. Ernzerhof, Hybrid Functionals Based on a Screened Coulomb Potential, J. Chem. Phys. 118(18) (2003) 8207-8215.
[24] I.D. Prodan, G.E. Scuseria, R.L. Martin, Covalency in the Actinide Dioxides: Systematic Study of the Electronic Properties using Screened Hybrid Density Functional Theory, Phys. Rev. B 76(3) (2007) 033101.
[25] M.E. Hoover, R. Atta-Fynn, A.K. Ray, Surface Properties of Uranium Dioxide from First Principles, J. Nucl. Mater. 452(1) (2014) 479-485.
[26] A. Georges, G. Kotliar, W. Krauth, M.J. Rozenberg, Dynamical Mean-Field Theory of Strongly Correlated Fermion Systems and the Limit of Infinite Dimensions, Rev. Mod. Phys. 68(1) (1996) 13.
[27] S.A. Moten, R. Atta-Fynn, A.K. Ray, M.N. Huda, Size Effects on the Electronic and Magnetic Properties of PuO_2 (111) Surface, J. Nucl. Mater. 468 (2016) 37-45.
[28] G. van der Laan, K.T. Moore, J.G. Tobin, B.W. Chung, M.A. Wall, A.J. Schwartz, Applicability of the Spin-Orbit Sum Rule for the Actinide 5f States, Phys. Rev. Lett. 93(9) (2004) 097401.
[29] R. Caciuffo, N. Magnani, P. Santini, S. Carretta, G. Amoretti, E. Blackburn, M. Enderle, P.J. Brown, G.H. Lander, Anisotropic magnetic fluctuations in 3-k antiferromagnets, J. Magn. Magn. Mater. 310(2, Part 2) (2007) 1698-1702.
[30] P. Giannozzi, P. Erdös, Theoretical analysis of the 3-k magnetic structure and distortion of uranium dioxide, J. Magn. Magn. Mater. 67(1) (1987) 75-87.
[31] C. Zhang, Y. Yang, P. Zhang, Water dissociation on the reduced PuO_2(110) surface from first principles, Science China Physics, Mechanics & Astronomy 62(10) (2019) 107002.
[32] H. Yu, G. Li, H. Li, R. Qiu, H. Huang, D. Meng, Adsorption and dissociation of H_2 on PuO_2 (110) surface: A density functional theory study, J. Alloys Compd. 654 (2016) 567-573.
[33] H. Yu, T. Tang, S. Zheng, Y. Shi, R. Qiu, W. Luo, D. Meng, A theoretical study of hydrogen atoms adsorption and diffusion on PuO_2 (110) surface, J. Alloys Compd. 666 (2016) 287-291.
[34] B. Ao, R. Qiu, H. Lu, P. Chen, Differences in the Existence States of Hydrogen in UO_2 and PuO_2 from DFT+U Calculations, J. Phys. Chem. C 120(33) (2016) 18445-18451.
[35] B. Ao, R. Qiu, G. Zhang, Z. Pu, X. Wang, P. Shi, Light impurity atoms as the probes for the electronic structures of actinide dioxides, Comput. Mater. Sci. 142 (2018) 25-31.
[36] T. Bo, J.-H. Lan, C.-Z. Wang, Y.-L. Zhao, C.-H. He, Y.-J. Zhang, Z.-F. Chai, W.-Q. Shi, First-Principles Study of Water Reaction and H_2 Formation on UO_2 (111) and (110) Single Crystal Surfaces, J. Phys. Chem. C 118(38) (2014) 21935-21944.
[37] T. Bo, J.-H. Lan, Y.-L. Zhao, Y.-J. Zhang, C.-H. He, Z.-F. Chai, W.-Q. Shi, Surface Properties of NpO_2 and Water Reacting with Stoichiometric and Reduced NpO_2 (111), (110), and (100) Surfaces From Ab Initio Atomistic Thermodynamics, Surf. Sci. 644 (2016) 153-164.
[38] T. Bo, J.-H. Lan, Y.-L. Zhao, Y.-J. Zhang, C.-H. He, Z.-F. Chai, W.-Q. Shi, First-Principles Study of Water Adsorption and Dissociation on the UO_2 (111), (110) and (100) Surfaces, J. Nucl. Mater. 454(1) (2014) 446-454.
[39] B.E. Tegner, M. Molinari, A. Kerridge, S.C. Parker, N. Kaltsoyannis, Water Adsorption on AnO2 {111}, {110}, and {100} Surfaces (An = U and Pu): A Density Functional Theory + U Study, J. Phys. Chem. C 121(3) (2017) 1675-1682.
[40] J.M. Flitcroft, M. Molinari, N.A. Brincat, M.T. Storr, S.C. Parker, Hydride ion formation in stoichiometric UO2, Chem. Commun. 51(90) (2015) 16209-16212.
[41] Joseph M. Flitcroft, M. Molinari, N.A. Brincat, N.R. Williams, M.T. Storr, G.C. Allen, S.C. Parker, The critical role of hydrogen on the stability of oxy-hydroxyl defect clusters in uranium oxide, J. Mater. Chem. A 6(24) (2018) 11362-11369.

[42] J. Glascott, A model for the initiation of reaction sites during the uranium–hydrogen reaction assuming enhanced hydrogen transport through linear oxide discontinuities, Philos. Mag. 94(13) (2014) 1393-1413.
[43] J. Glascott, A model for the initiation of reaction sites during the uranium–hydrogen reaction assuming enhanced hydrogen transport through thin areas of surface oxide, Philos. Mag. 94(3) (2014) 221-241.
[44] M. Fronzi, S. Piccinin, B. Delley, E. Traversa, C. Stampfl, Water adsorption on the stoichiometric and reduced CeO2(111) surface: a first-principles investigation, Phys. Chem. Chem. Phys. 11(40) (2009) 9188-9199.
[45] J.T. Pegg, A.E. Shields, M.T. Storr, D.O. Scanlon, N.H. de Leeuw, Interaction of Hydrogen with Actinide Dioxide (111) Surfaces, The Journal of Chemical Physics 150(13) (2019) 134701.
[46] V.I. Anisimov, Strong Coulomb Correlations in Electronic Structure Calculations, CRC Press2000.
[47] J. Heyd, G.E. Scuseria, M. Ernzerhof, Erratum:"Hybrid functionals based on a screened Coulomb potential"[J. Chem. Phys. 118, 8207 (2003)], The Journal of Chemical Physics 124(21) (2006) 219906.
[48] G.I. Csonka, J.P. Perdew, A. Ruzsinszky, P.H. Philipsen, S. Lebègue, J. Paier, O.A. Vydrov, J.G. Ángyán, Assessing the Performance of Recent Density Functionals for Bulk Solids, Phys. Rev. B 79(15) (2009) 155107.
[49] D. Hait, A. Rettig, M. Head-Gordon, Well-behaved versus ill-behaved density functionals for single bond dissociation: Separating success from disaster functional by functional for stretched H2, The Journal of Chemical Physics 150(9) (2019) 094115.
[50] G. Henkelman, A. Arnaldsson, H. Jónsson, A fast and robust algorithm for Bader decomposition of charge density, Comput. Mater. Sci. 36(3) (2006) 354-360.
[51] W. Tang, E. Sanville, G. Henkelman, A grid-based Bader analysis algorithm without lattice bias, J. Phys.: Condens. Matter 21(8) (2009) 084204.
[52] E. Sanville, S.D. Kenny, R. Smith, G. Henkelman, Improved grid-based algorithm for Bader charge allocation, J. Comput. Chem. 28(5) (2007) 899-908.
[53] A. Horn, H. Lanig, Encyclopedia of Computational Chemistry, Molecular modeling annual 5(9) (1999) 141-142.
[54] E. Bousquet, N. Spaldin, J-dependence in the LSDA+U Treatment of Noncollinear Magnets, Phys. Rev. B 82(22) (2010) 220402.
[55] M.T. Suzuki, N. Magnani, P.M. Oppeneer, Microscopic Theory of the Insulating Electronic Ground States of the Actinide Dioxides AnO_2 (An = U, Np, Pu, Am, and Cm), Phys. Rev. B 88(19) (2013) 195146.
[56] G.W. Watson, E.T. Kelsey, N.H. de Leeuw, D.J. Harris, S.C. Parker, Atomistic Simulation of Dislocations, Surfaces and Interfaces in MgO, J. Chem. Soc., Faraday Trans. 92(3) (1996) 433-438.
[57] P. Tasker, W., The Structure and Properties of Fluorite Crystal Surfaces, J. Phys. Colloques 41(C6) (1980) C6-488-C6-491.
[58] P.W. Tasker, The Stability of Ionic Crystal Surfaces, J. Phys. C: Solid State Phys. 12(22) (1979) 4977.
[59] W. Sun, G. Ceder, Efficient Creation and Convergence of Surface Slabs, Surf. Sci. 617 (2013) 53-59.
[60] S. Steiner, S. Khmelevskyi, M. Marsmann, G. Kresse, Calculation of the Magnetic Anisotropy with Projected-Augmented-Wave Methodology and the Case Study of Disordered $Fe_{1-x}Co_x$ Alloys, Phys. Rev. B 93(22) (2016) 224425.

[61] Alex M. Ganose, Adam J. Jackson, D.O. Scanlon, sumo: Command-line tools for plotting and analysis of periodic ab initio calculations, Journal of Open Source Software 3(28) (2018) 717.
[62] A. Balakrishnan, V. Smith, B.P. Stoicheff, Dissociation energy of the hydrogen molecule, Phys. Rev. Lett. 68(14) (1992) 2149-2152.
[63] G. Herzberg, The dissociation energy of the hydrogen molecule, J. Mol. Spectrosc. 33(1) (1970) 147-168.
[64] J.M. Haschke, T.H. Allen, Plutonium Hydride, Sesquioxide and Monoxide Monohydride: Pyrophoricity and Catalysis of Plutonium Corrosion, J. Alloys Compd. 320(1) (2001) 58-71.
[65] J.M. Haschke, T.H. Allen, J.C. Martz, Oxidation Kinetics of Plutonium in Air: Consequences for Environmental Dispersal, J. Alloys Compd. 271–273 (1998) 211-215.
[66] D. Olander, Nuclear fuels – Present and future, J. Nucl. Mater. 389(1) (2009) 1-22.
[67] Y. Tanaka, N. Terada, T. Nakajima, M. Taguchi, T. Kojima, Y. Takata, S. Mitsuda, M. Oura, Y. Senba, H. Ohashi, S. Shin, Incommensurate Orbital Modulation behind Ferroelectricity in ${\mathrm{CuFeO}}_{2}$, Phys. Rev. Lett. 109(12) (2012) 127205.
[68] T.M. McCleskey, E. Bauer, Q. Jia, A.K. Burrell, B.L. Scott, S.D. Conradson, A. Mueller, L. Roy, X. Wen, G.E. Scuseria, Optical band gap of NpO_2 and PuO_2 from optical absorbance of epitaxial films, J. Appl. Phys. 113(1) (2013) 013515.
[69] P. Erdös, G. Solt, Z. ⊙ołnierek, A. Blaise, J.M. Fournier, Magnetic Susceptibility and the Phase Transition of NpO_2, Physica B+C 102(1) (1980) 164-170.

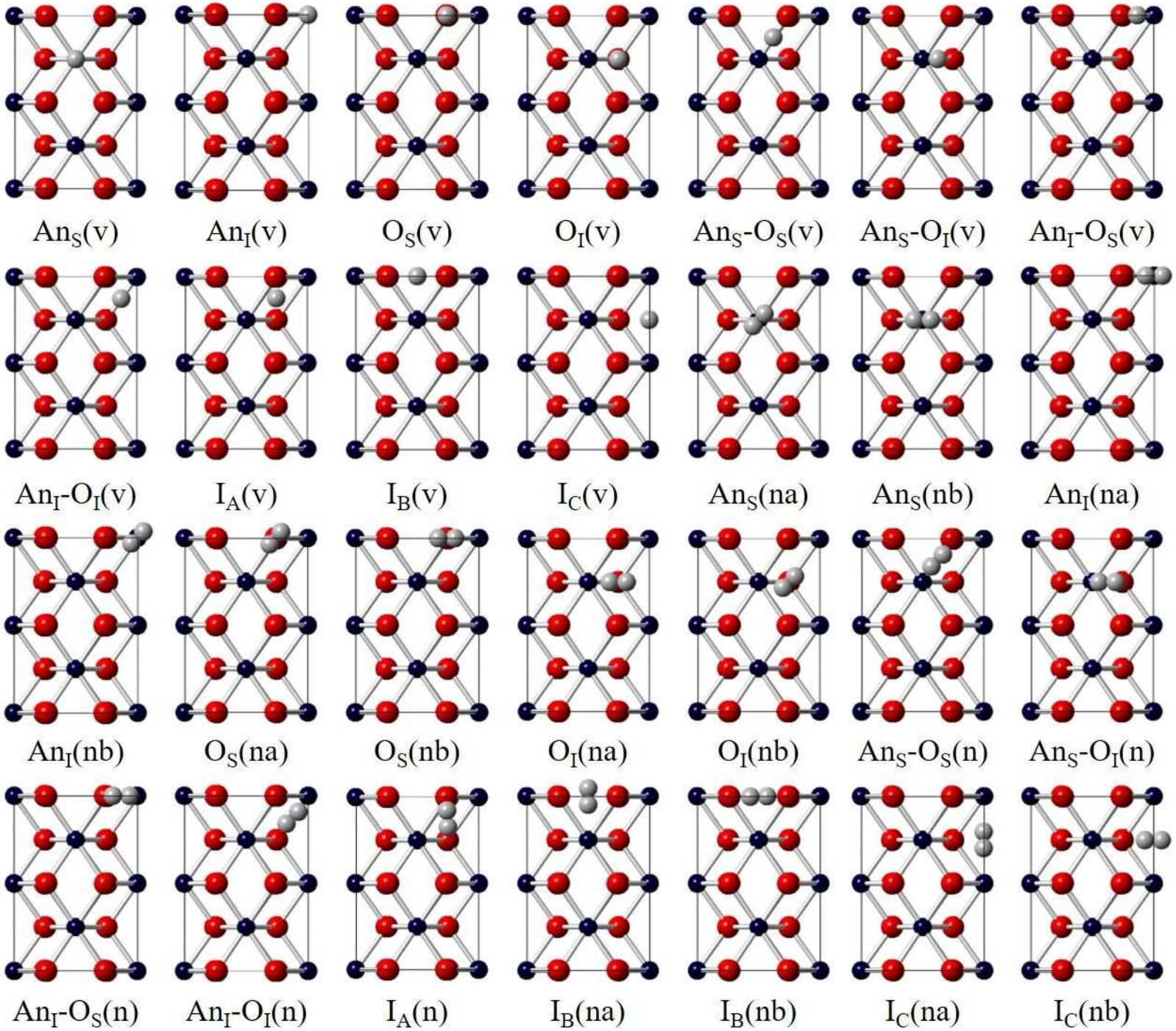
$An_S(v)$
$An_I(v)$
$O_S(v)$
$O_I(v)$
An_S-$O_S(v)$
An_S-$O_I(v)$
An_I-$O_S(v)$
An_I-$O_I(v)$
$I_A(v)$
$I_B(v)$
$I_C(v)$
$An_S(na)$
$An_S(nb)$
$An_I(na)$
$An_I(nb)$
$O_S(na)$
$O_S(nb)$
$O_I(na)$
$O_I(nb)$
An_S-$O_S(n)$
An_S-$O_I(n)$
An_I-$O_S(n)$
An_I-$O_I(n)$
$I_A(n)$
$I_B(na)$
$I_B(nb)$
$I_C(na)$
$I_C(nb)$

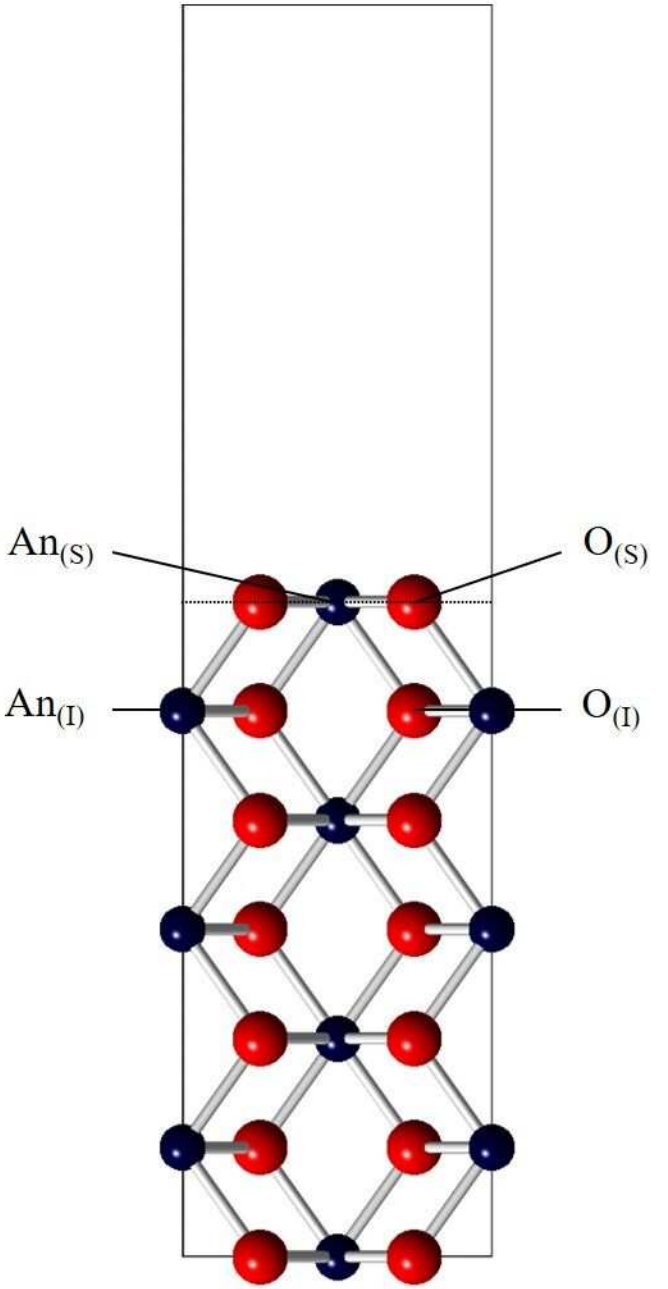
$An_{(S)}$
$O_{(S)}$
$An_{(I)}$
$O_{(I)}$

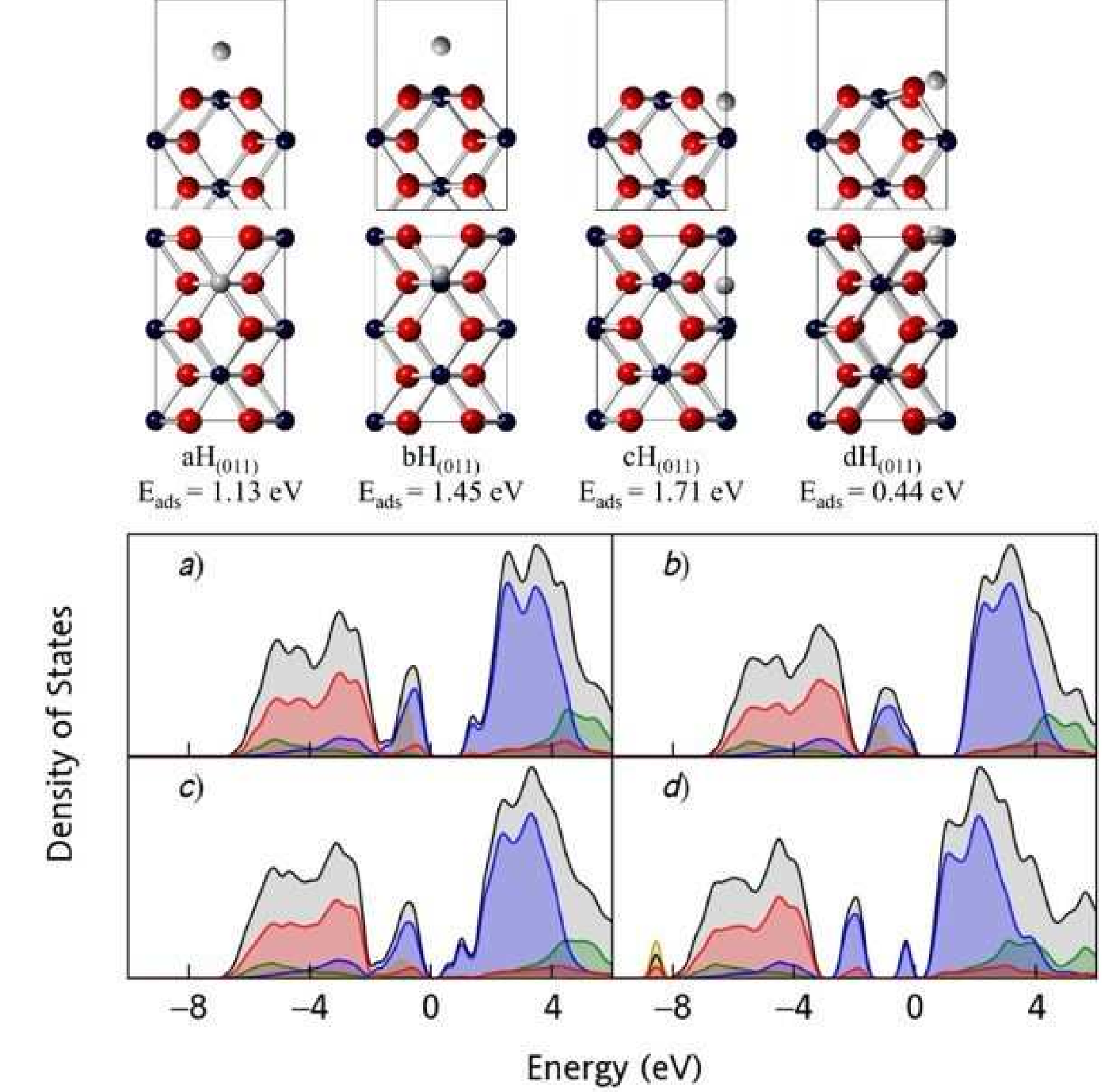
aH(011)
Eads = 1.13 eV
bH(011)
Eads = 1.45 eV
cH(011)
Eads = 1.71 eV
dH(011)
Eads = 0.44 eV
a)
b)
c)
d)
Density of States
−8
−4
0
4
−8
−4
0
4
Energy (eV)

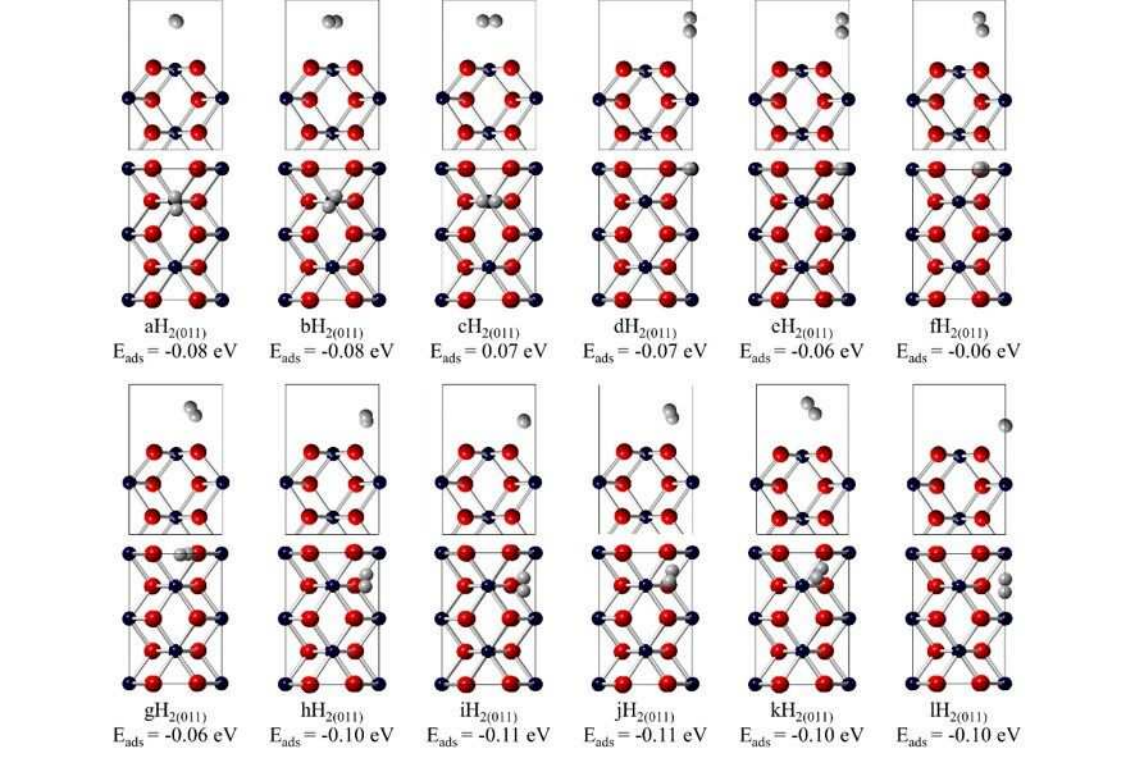
aH2(011)
Eads = -0.08 eV
bH2(011)
Eads = -0.08 eV
cH2(011)
Eads = 0.07 eV
dH2(011)
Eads = -0.07 eV
eH2(011)
Eads = -0.06 eV
fH2(011)
Eads = -0.06 eV
gH2(011)
Eads = -0.06 eV
hH2(011)
Eads = -0.10 eV
iH2(011)
Eads = -0.11 eV
jH2(011)
Eads = -0.11 eV
kH2(011)
Eads = -0.10 eV
lH2(011)
Eads = -0.10 eV

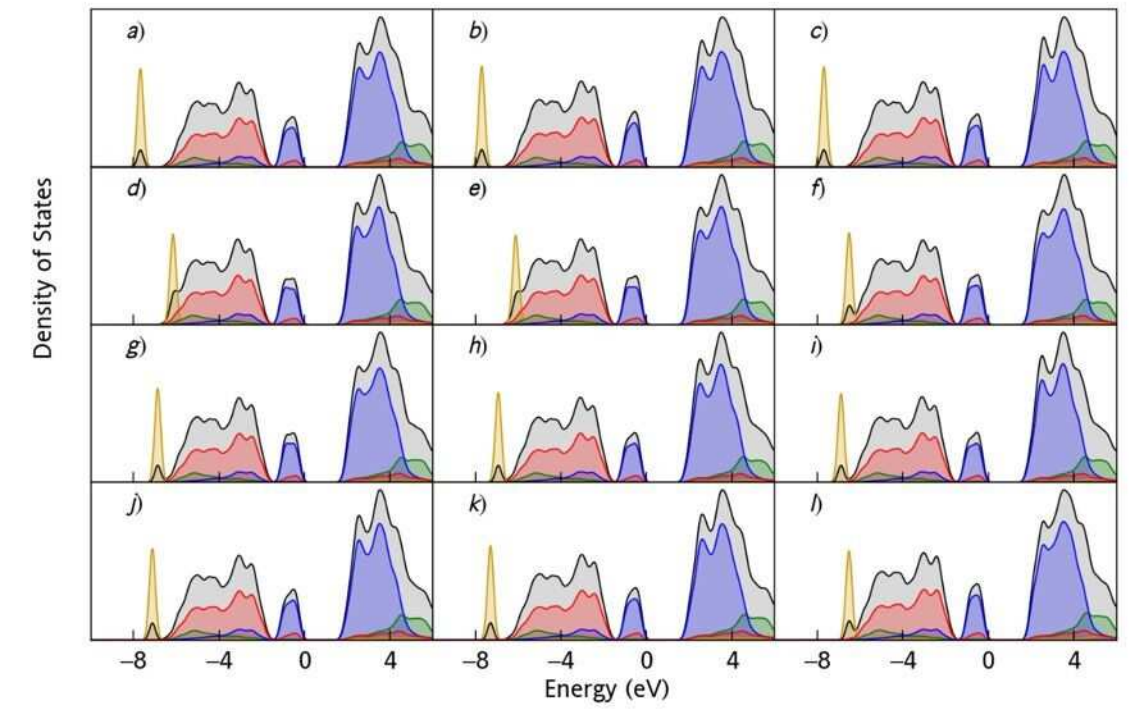
a)
b)
c)
d)
e)
f)
g)
h)
i)
j)
k)
l)
Density of States
−8
−4
0
4
Energy (eV)

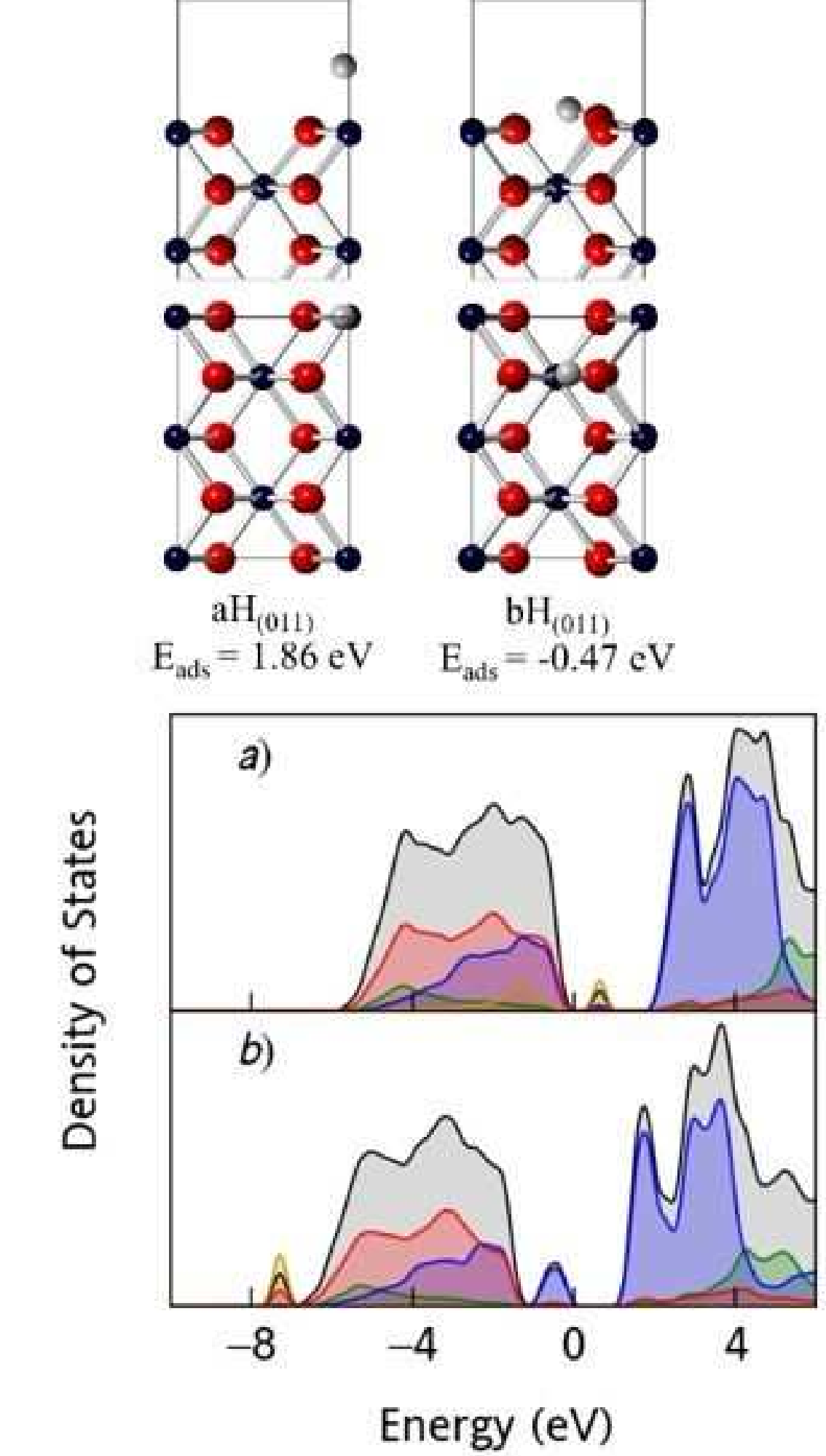
aH(011)
Eads = 1.86 eV
bH(011)
Eads = -0.47 eV
a)
b)
Density of States
−8
−4
0
4
Energy (eV)

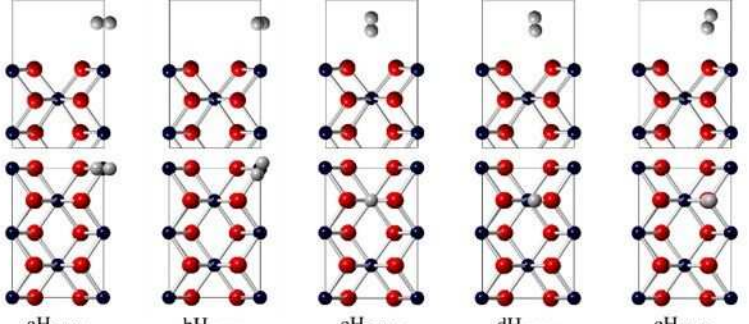

$aH_{2(011)}$ E_{ads} = -0.08 eV
$bH_{2(011)}$ E_{ads} = -0.07 eV
$cH_{2(011)}$ E_{ads} = -0.07 eV
$dH_{2(011)}$ E_{ads} = -0.07 eV
$eH_{2(011)}$ E_{ads} = -0.06 eV

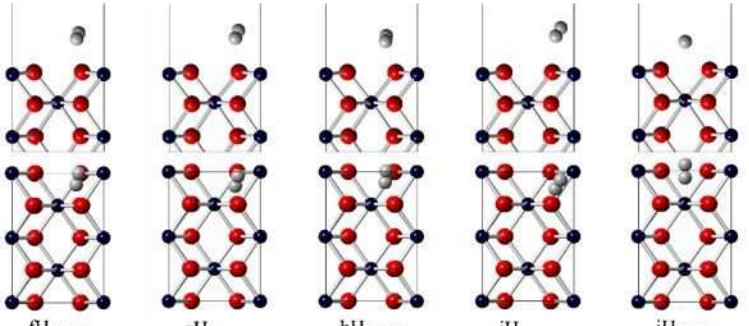

$fH_{2(011)}$ E_{ads} = -0.10 eV
$gH_{2(011)}$ E_{ads} = -0.10 eV
$hH_{2(011)}$ E_{ads} = -0.10 eV
$iH_{2(011)}$ E_{ads} = -0.10 eV
$jH_{2(011)}$ E_{ads} = -0.09 eV

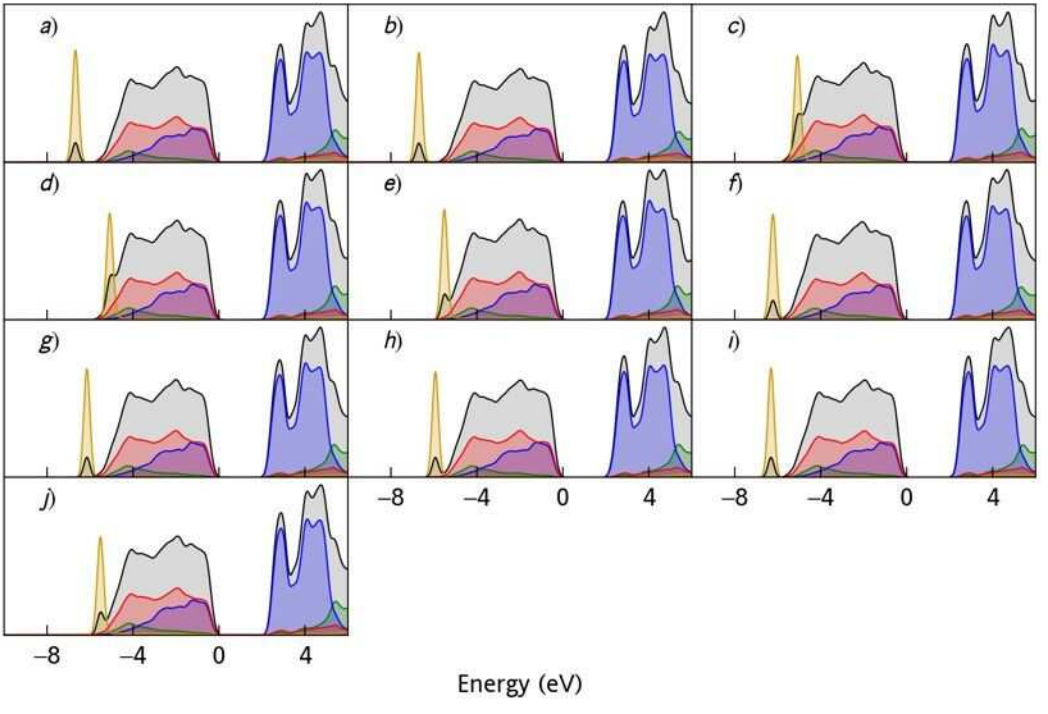

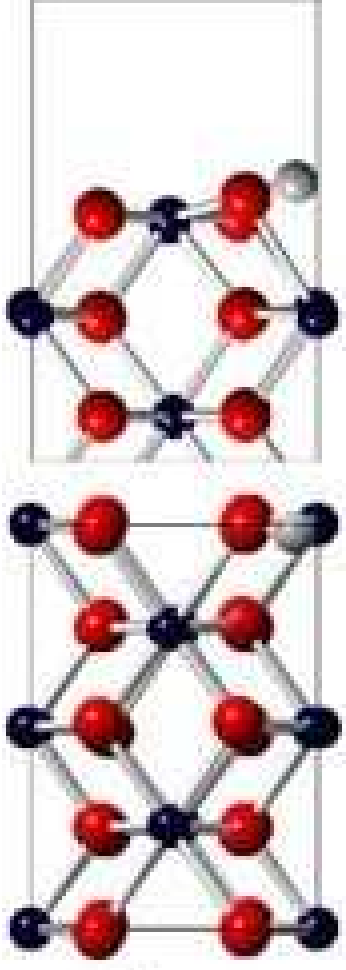

$aH_{(011)}$

E_{ads} = -1.71 eV

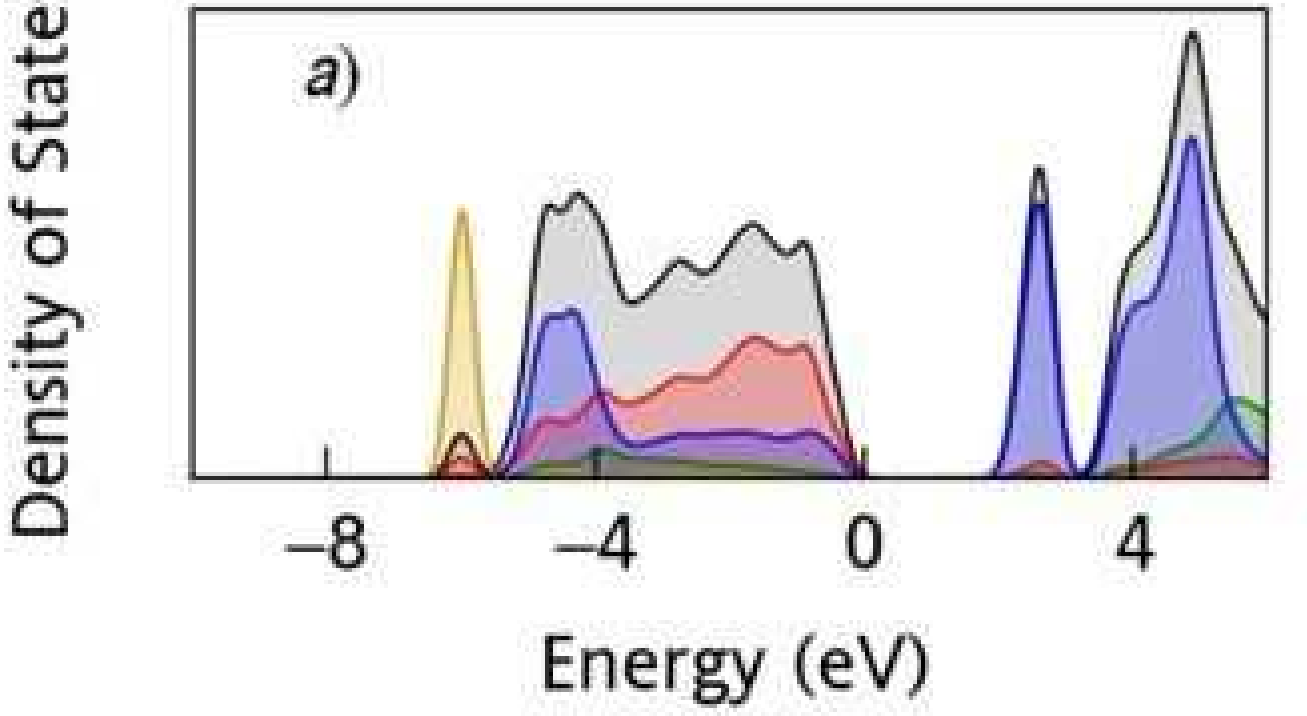

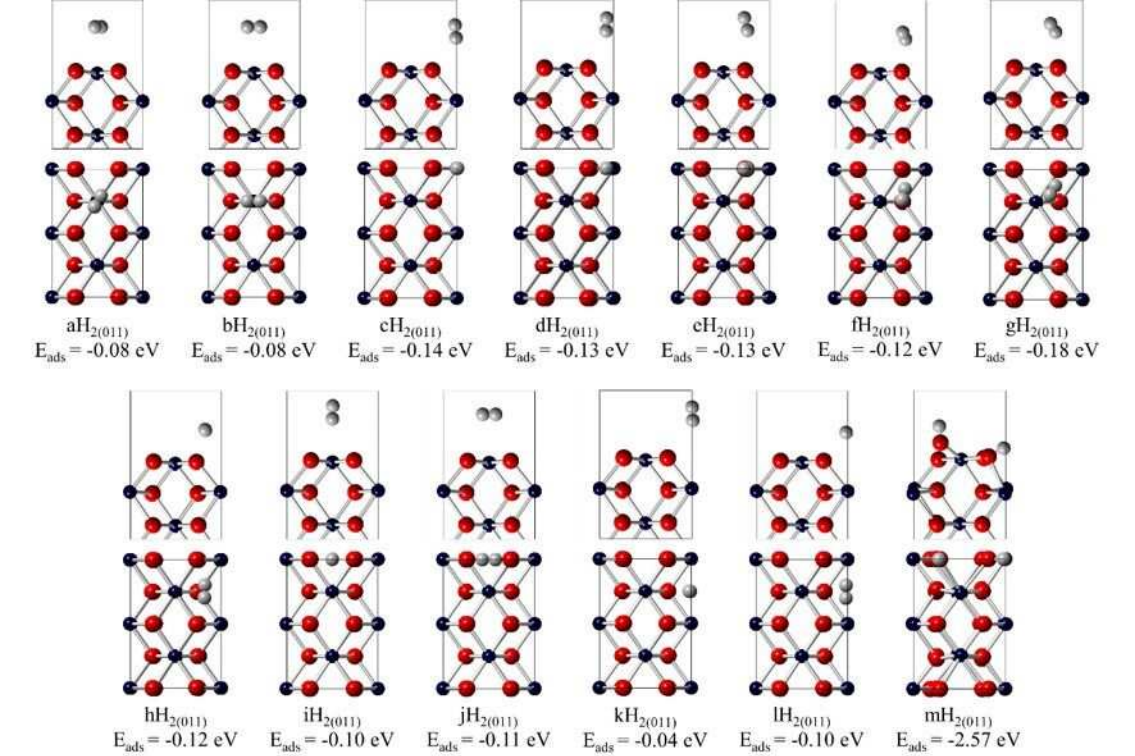
aH2(011)
Eads = -0.08 eV
bH2(011)
Eads = -0.08 eV
cH2(011)
Eads = -0.14 eV
dH2(011)
Eads = -0.13 eV
eH2(011)
Eads = -0.13 eV
fH2(011)
Eads = -0.12 eV
gH2(011)
Eads = -0.18 eV
hH2(011)
Eads = -0.12 eV
iH2(011)
Eads = -0.10 eV
jH2(011)
Eads = -0.11 eV
kH2(011)
Eads = -0.04 eV
lH2(011)
Eads = -0.10 eV
mH2(011)
Eads = -2.57 eV

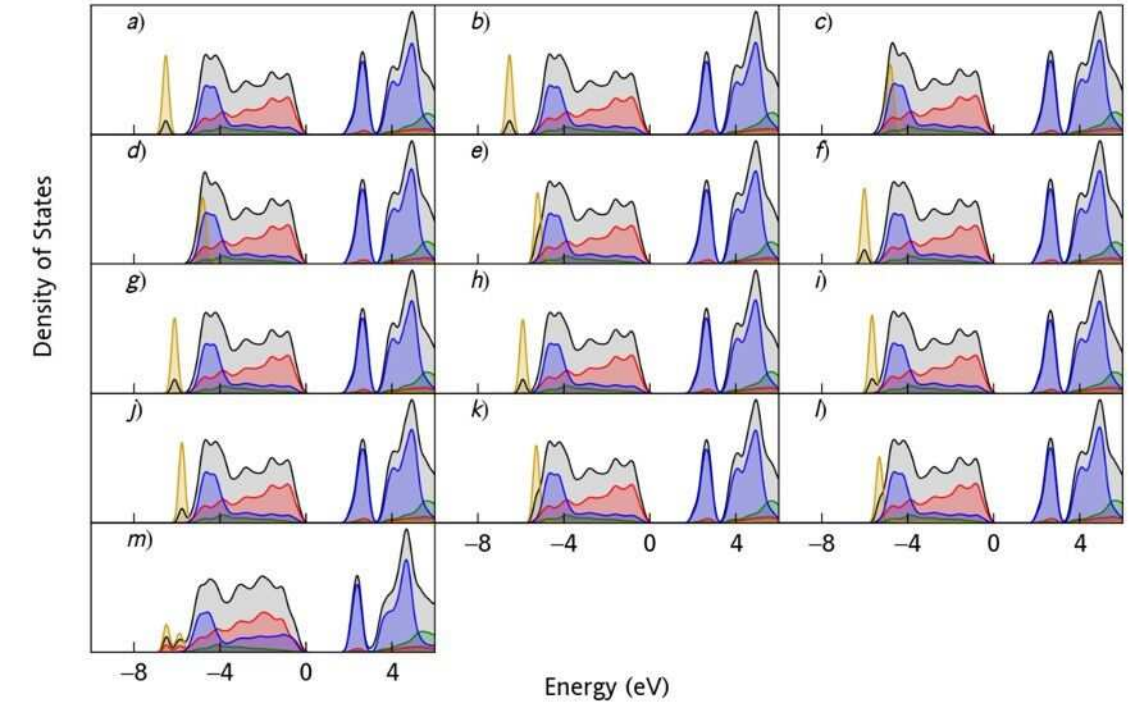
a)
b)
c)
d)
e)
f)
g)
h)
i)
j)
k)
l)
m)
Density of States
−8
−4
0
4
Energy (eV)